RESEARCH ARTICLE | SEPTEMBER 30 2025

# Structured light approaches in laser-based plasma diagnostics

Special Collection: Papers from the 66th Annual Meeting of the APS Division of Plasma Physics

Ivan Romadanov 🖾 🗓 ; Yevgeny Raitses 🗓



Phys. Plasmas 32, 093513 (2025) https://doi.org/10.1063/5.0281099





### Articles You May Be Interested In

Confocal laser induced fluorescence with comparable spatial localization to the conventional method

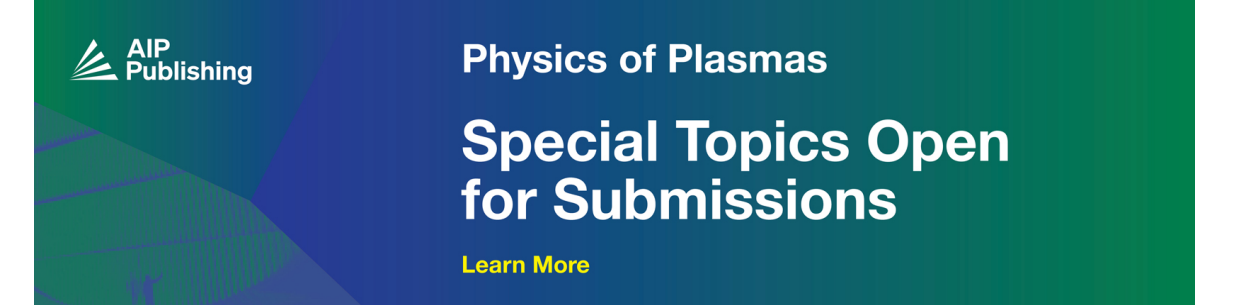
Rev. Sci. Instrum. (October 2017)

Anti-contamination SMART (Spectrum Monitoring Apparatus with Roll-to-roll Transparent film) window for optical diagnostics of plasma systems

Rev. Sci. Instrum. (January 2021)

Scattering characteristics of multiple Bessel vortex beams by transverse plasma flows

Phys. Plasmas (March 2025)





# Structured light approaches in laser-based plasma diagnostics

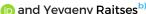
Cite as: Phys. Plasmas 32, 093513 (2025); doi: 10.1063/5.0281099 Submitted: 16 May 2025 · Accepted: 10 September 2025 · Published Online: 30 September 2025

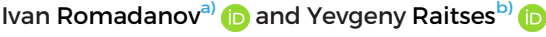












#### **AFFILIATIONS**

Princeton Plasma Physics Laboratory, Princeton, NJ 08543, USA

Note: This paper is part of the Special Collection: Papers from the 66th Annual Meeting of the APS Division of Plasma Physics. Note: Paper QI3 4, Bull. Am. Phys. Soc. 70 (2025).

alnvited speaker. Author to whom correspondence should be addressed: iromada2@pppl.gov

#### **ABSTRACT**

There is a growing demand for plasma diagnostics suitable for industrial plasma reactors employed in semiconductor nanofabrication, especially relevant to microelectronics and quantum information systems. Such reactors typically have limited optical access and pose considerable diagnostic challenges, including intense background emission, significant thermal loads, and contamination of optical viewports. In this study, we outline research into structured light techniques (laser beams with tailored spatial, temporal, or phase characteristics) that effectively overcome these issues using laser-induced fluorescence (LIF) as an example. The focus of presented diagnostics is on ion kinetics analysis within an industrial plasma source, although this approach is broadly applicable to other plasma systems and diagnostic contexts. We present a confocal LIF implementation using an axicon-generated Bessel annular beam, achieving spatial resolutions of approximately 5 mm at a focal distance of 300 mm, with potential improvements to about 1 mm. This approach matches conventional orthogonal LIF performance but requires only one optical port. Wavelength-modulation LIF employs nonlinear laser wavelength tuning to measure spectral line derivatives, suppressing background emission and enhancing details of spectral line shape. Additionally, we present new results on applying vortex beams (laser beams carrying orbital angular momentum, OAM) for LIF measurements in an industrial plasma device. These measurements enable simultaneous axial and tangential velocity determination using a single laser beam and have been tested with xenon ion transition. Initial quantification of results was performed. Together, these structured-light approaches provide robust, background-resilient, multi-dimensional diagnostics for complex plasma environments.

© 2025 Author(s). All article content, except where otherwise noted, is licensed under a Creative Commons Attribution (CC BY) license (https:// creativecommons.org/licenses/by/4.0/). https://doi.org/10.1063/5.0281099

#### I. INTRODUCTION

Optical diagnostics are essential tools for plasma research, providing direct, in situ measurements of plasma properties.<sup>1,2</sup> Laser-based diagnostics<sup>3</sup> represent a significant subset, utilizing laser beams to interact selectively with specific plasma species like electrons, atoms, ions, or molecules. Analyzing the resulting scattered light, absorption, or fluorescence yields detailed species-specific information with high spatial and in some cases temporal resolution. Common methods include Thomson scattering,<sup>5</sup> laser absorption spectroscopy,<sup>6,7</sup> and laser-induced fluorescence.8 These techniques are widely applied in fundamental plasma studies (e.g., plasma-wall interactions, 9,10 fusion experiments<sup>11</sup>) and applied research like electric propulsion<sup>12</sup> and industrial plasma processing. 13,14

Industrial plasma reactors used in semiconductor fabrication need advanced in situ diagnostics for better understanding of physical processed or real time control<sup>15-20</sup> yet transferring laboratory tools into these chambers is challenging. 21 The reactors contain hazardous gases, operate over wide temperature ranges, and have opaque conductive or dielectric walls that block light. Because these walls control the discharge through plasma-surface interactions, 22,23 adding new viewports could disrupt the process. Intense emission from arcs or hot filaments masks weak diagnostic signals. Safety constraints often require placement of optics and detectors far from the chamber, although high selectivity and spatial resolution must be maintained. Any diagnostic for this setting must therefore work through restricted or indirect sight-lines, reject strong background emission, and maintain highresolution performance at a distance. Additionally, conventional laser diagnostics probe plasma only along the beam axis, so they miss anisotropic effects such as ion motion parallel and perpendicular to surfaces. Alternative methods are needed that could provide multi-dimensional

b) Electronic mail: yraitses@pppl.gov

data from a single beam. Such diagnostics would significantly surpass the capabilities of simpler, bulk-averaged methods like optical emission spectroscopy (OES).<sup>24–27</sup> Moreover, such diagnostics would generate data for validating computational codes and developing physics-informed machine learning techniques. Although industry drives this development, the resulting techniques will also expand experimental capability in laboratory plasmas beyond bulk-averaged tools like optical emission spectroscopy.

Laser-induced fluorescence (LIF) is the main diagnostic examined in this paper and is considered as a standard tool for measuring ions, neutral atoms, and molecules in low-temperature plasmas. In LIF, a laser is tuned to a specific atomic or ionic transition and illuminates the plasma; the excited species then emit fluorescence as they relax to lower energy states. By scanning the laser wavelength across the chosen line, one records a fluorescence spectrum whose Doppler shift reveals particle flow velocity, while its linewidth reflects particle temperature and energy spread. Because LIF is highly sensitive, species-selective, and only weakly intrusive, it can track plasma dynamics in real time without noticeably disturbing the discharge.

In this paper, we explore structured light<sup>28</sup> techniques within the context of LIF diagnostics. Structured light refers to laser beams engineered by shaping spatial intensity, phase, polarization, temporal, or frequency properties. Optical vortex beams<sup>29</sup> are a prominent example and have enabled advances in optical communications, 30 micromanipulation, quantum information, and super-resolution imaging. Yet, the potential of structured light beams for plasma diagnostics is largely unexplored with only a few recent examples. 32,33 While our examples focus on LIF, the challenges addressed—limited optical access, strong background noise, and the need for more complex, multidimensional measurements from a single beam—are broadly relevant to other laser-based plasma diagnostics. We present three structured-light approaches, each targeting one of these key limitations: (1) confocal LIF employing structured annular beams to overcome limited optical access; 34 (2) wavelength-modulation LIF to effectively extract complex velocity distribution function (VDF) shapes from noise environment;<sup>35</sup> and (3) vortex-beam-based LIF to enable two-dimensional (2D) VDF measurements using only a single laser beam.3

This paper is organized as follows: Sec. II introduces basic principles of LIF diagnostics. Section III demonstrates practical implementations and advantages of structured-light techniques, detailing results obtained from confocal, wavelength-modulation, and vortex-beam LIF experiments. Section IV describes the experimental setups and LIF arrangement for conventional and vortex LIF setups. Section V briefly describes the results obtained. Finally, Sec. VI summarizes the paper and provides an outlook on future developments and broader applications of structured-light diagnostics in plasma research and industrial settings.

# II. DOPPLER SHIFT BASED LASER INDUCED FLUORESCENCE

Laser-induced fluorescence (LIF) spectroscopy is a minimally perturbative optical diagnostic technique widely used in plasma physics to obtain spatially and temporally resolved measurements of key plasma properties. In this method, a tunable laser is set to match a resonant transition of a selected plasma species—such as atoms, ions, or molecules. Since the laser wavelength is tuned to a specific electronic transition, LIF provides highly selective, species-specific measurements. Only those particles that satisfy the resonance condition will absorb the laser photons and be excited to a higher electronic state. The excited species then decay spontaneously, emitting fluorescence photons that can be detected. LIF can be used to measure population densities in specific quantum states and VDFs, which contain information about temperatures, flow velocities, or electric fields or ionization collisions.<sup>37,38</sup> In some cases, electric and magnetic fields can also be directly determined through Stark<sup>39</sup> and Zeeman<sup>40–42</sup> effects, respectively. The description below refers specifically to excitation by singlephoton absorption, commonly known as single-photon LIF. Excitation through multi-photon absorption is also possible, although it is not considered here; see Refs. 43 and 44 for further discussion.

In practical implementations of LIF, the laser most often excites particles from a metastable state—a long-lived excited level populated in the plasma primarily through collisions with electrons. These metastable states generally have sufficient population in low-temperature plasmas and feature transition wavelengths accessible with commercially available lasers. To obtain ground-state properties from measurements of metastable populations, one must assume thermal or collisional equilibrium between these states. Examples of two LIF transitions for Ar<sup>+10,45</sup> and Xe<sup>+46,47</sup> that were used in this work are shown in Figs. 1(a) and 1(b).

Laser excitation must obey standard quantum selection rules, <sup>48</sup> which depend on angular momentum coupling schemes and transition multipole types (e.g., electric dipole, quadrupole). Although "forbidden" transitions can occur through higher-order processes such as magnetic dipole or electric quadrupole mechanisms, their rates are typically too low to produce detectable fluorescence signals under standard conditions. After excitation, the upper state can decay to the lower level either resonantly (returning to the original state) or non-resonantly (decaying to a different state). Non-resonant fluorescence is generally preferred, as it occurs at a wavelength different from the excitation laser, simplifying detection by reducing background interference. The detected fluorescence intensity is directly proportional to the population of the initial (excited) state and depends on several physical and instrumental parameters. In the weak laser intensity limit, the fluorescence signal depends on: (1) the upper state lifetime, including radiative and quenching

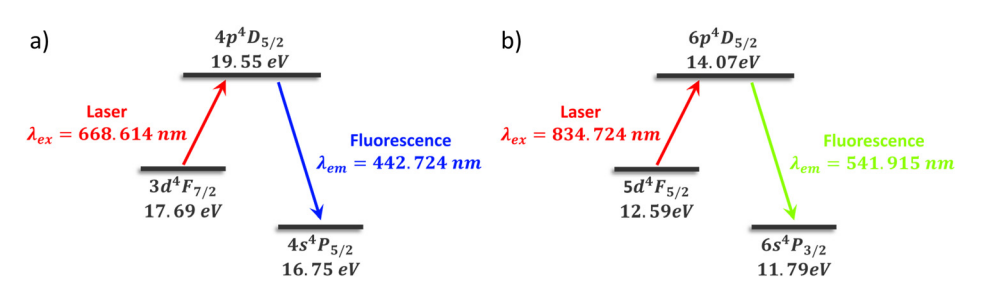


**FIG. 1.** Laser-induced fluorescence (LIF) excitation schemes for  $Ar^+$  (a) and  $Xe^+$  (b) metastable states. All wavelengths are given in vacuum. Energy levels and transition data are based on NIST Atomic Spectra Database. Diagrams are not to scale.

contributions; (2) the absorption cross section; (3) the initial density of the probed state; (4) the spectral overlap between the laser and absorption line profiles; and (5) the laser photon flux. When these factors are properly characterized and calibrated, LIF enables both relative and absolute measurements of population densities.

One of the important properties that can be inferred from LIF measurements is the VDF. The VDF is central to understanding a plasma's thermodynamic state, as it contains information about the temperature, mean (bulk) velocity, and most probable velocity of the plasma species. In cases where the distribution deviates from Maxwellian—such as with energetic tails—it can also provide insights into physical processes like charge exchange or electric field. The fundamental principle is that moving particles perceive the laser frequency as shifted from resonance due to the Doppler effect. As illustrated in Fig. 2, only those particles whose velocity component along the laser beam wavevector k matches the Doppler-shifted resonance condition will absorb the light [Fig. 2(a)]. After excitation, they de-excite and emit fluorescence photons [Fig. 2(b)]. Particles with other velocities remain off resonance and are not excited [Fig. 2(c)].

Quantitatively, consider a particle (ion or atom) moving at velocity v in the laboratory frame. The laser frequency  $\omega$  in the lab frame is seen by the particle as  $\omega' = \omega + \mathbf{k} \cdot \mathbf{v}$ . For the particle to absorb the photon,  $\omega'$  must equal the transition frequency  $\omega_0$ ,

$$\omega - \omega_0 = -\mathbf{k} \cdot \mathbf{v}. \tag{1}$$

A positive Doppler shift  $(\mathbf{k} \cdot \mathbf{v} < 0)$  corresponds to a blue shift (particle moving opposite to  $\mathbf{k}$ , increasing absorption frequency), while a negative shift  $(\mathbf{k} \cdot \mathbf{v} > 0)$  corresponds to a red shift (particle is moving opposite to  $\mathbf{k}$ , decreasing absorption frequency). This means that the laser should be tuned to lower frequencies (red shifted) to detect particles moving toward the laser, and to higher frequencies (blue shifted) when detecting particles moving away from the laser.

Because particles in the plasma have a range of velocities, the absorption line becomes Doppler-broadened. By scanning the laser frequency across this broadened line and recording the fluorescence signal at each point, one obtains a velocity-resolved signal that directly

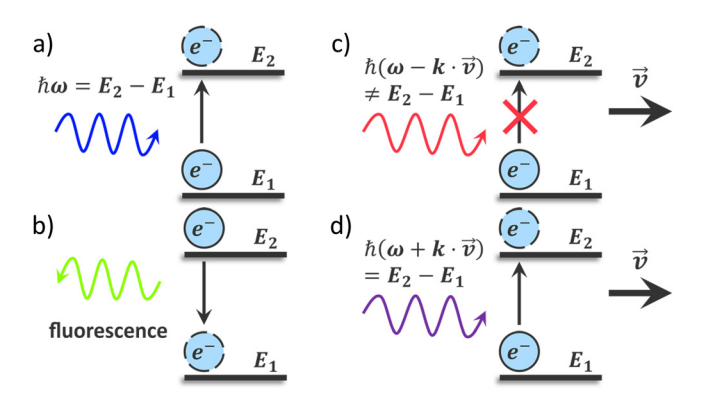


**FIG. 2.** Schematic illustration of Doppler-shift-based LIF. (a) A stationary particle absorbs laser light when the incoming photon frequency matches the resonant transition, leading to excitation. (b) The excited particle subsequently decays and emits a fluorescence photon. (c) A particle moving away from the laser source perceives the laser light as red-shifted and does not absorb it, so no excitation occurs. (d) General case for a particle with velocity matching the Doppler-shifted resonance condition. Only such particles will contribute to the LIF signal.

reconstructs the VDFs profile. The full velocity distribution is measured, not just average quantities. From these data, important plasma parameters can be extracted. For example, the ion temperature is related to the width of the Doppler-broadened profile (wider distribution implies higher thermal speeds), and the mean flow velocity is indicated by the shift of the distribution's centroid (if the whole VDF is displaced from zero velocity). In a Maxwellian plasma, the fluorescence line shape is roughly Gaussian, whose width yields the temperature and whose centroid shift yields the bulk flow or drift speed. Moreover, measured VDFs provide rich thermodynamic information about plasma: one can determine not only temperature and flow, but also detect non-Maxwellian features, velocity-space diffusion, or multiple populations. The ability to obtain time-resolved and spatially resolved VDFs allows detailed studies of plasma kinetics and transport.

An example of ion VDF (IVDF) obtained for argon ion in system described in Sec. IV is shown in Fig. 3. Fitting with a Maxwellian distribution is performed and flow velocity and temperature of the population are extracted. It is important to emphasize that post-processing of LIF results—particularly the reconstruction of the VDF—requires careful consideration of factors beyond Doppler broadening. While the Doppler effect dominates the line shape in many cases, other effects—such as Zeeman splitting, power broadening, collisional broadening, and saturation<sup>3,49</sup>—can significantly alter the fluorescence profile. These contributions depend on parameters like applied magnetic field strength, laser power, background pressure, and collisional environment. If not properly accounted for, they may distort the measured VDF and lead to nonphysical interpretations. Accurate analysis must therefore include correction for these effects to ensure reliable extraction of plasma parameters.

#### III. STRUCTURED LIGHT

Structured light<sup>28,50</sup> describes laser beams whose spatial, temporal, or phase profile is specifically engineered, in contrast to the

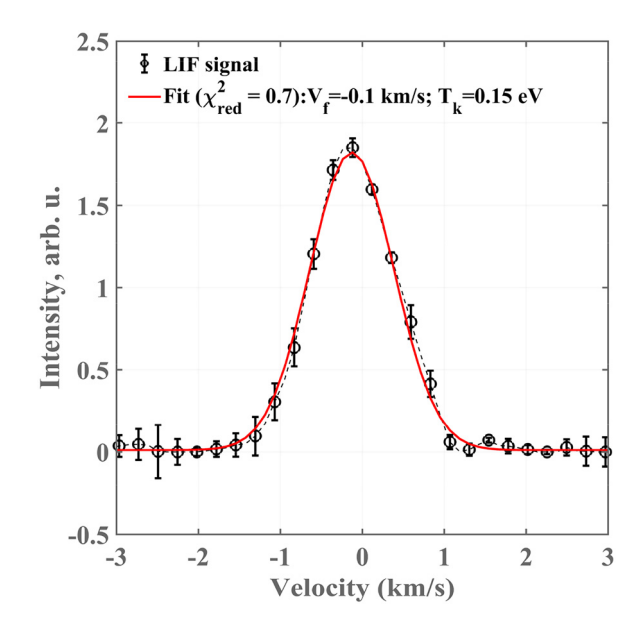


**FIG. 3.** Example of IVDF shape obtained for argon ions. Fitting is performed with a Maxwellian function with  $\chi^2_{red}$  used as a goodness of measure and flow velocities and temperatures are estimated.

Gaussian (TEM<sub>00</sub>) mode. Such beams can be manipulated along many degrees of freedom-frequency, duration, complex amplitude, polarization, and full three-dimensional structure—to create rings (Bessel beams),<sup>51</sup> optical vortices with orbital angular momentum,<sup>52</sup> or patterns modulated in time or space.<sup>53</sup> These tailored fields provide new mechanisms in numerous optical techniques. Structured illumination and confocal microscopy<sup>54</sup> push resolution beyond the diffraction limit, spectroscopy, and other sensing tasks also benefit from the added control. 55,56 Vortex beams enable optical tweezers to trap, translate, and rotate microparticles with high precision.<sup>57</sup> In quantum optics and free-space communication, higher-order modes encode and multiplex information in high-dimensional Hilbert spaces, providing secure and efficient data transfer.<sup>58</sup> Despite their extensive applications across many fields, structured light is largely unexplored for plasma diagnostic. A few examples include planar sheets in LIF<sup>59</sup> or Airy beams in laser-induced breakdown spectroscopy. 60 Most measurements still rely on simple TEM<sub>00</sub> beams. Extending structured beams to plasma research promises advances for both fundamental science and industrial applications.

Structured light can be broadly categorized as spatially structured beams and spatiotemporal beams. A spatially structured beam has an inhomogeneous amplitude or phase profile at a fixed moment in time. These beams are classified based on the plane of their inhomogeneities: transverse beams (Hermite–Gaussian, Laguerre–Gaussian, Bessel, and vortex beams that carry orbital angular momentum, as well as radially or azimuthally polarized vector beams) or longitudinal beams (Airy beams with parabolic trajectories, Mathieu beams, winding beams with elliptical trajectories). Spatiotemporal beams extend the concept by linking spatial structure to a synchronized temporal modulation, producing patterns that change in both space and time. Conventional adjustments of a laser's amplitude or wavelength are not usually labeled structured light yet nonlinear modulation of these quantities can yield complex, tailored illumination that serves the same purpose.

Generation and characterization of structured light beams constitute actively developing research areas, closely linked to the expanding applications mentioned above. Spatial light modulators, <sup>63</sup> metasurfaces, <sup>64</sup> and holographic phase masks <sup>65</sup> are commonly utilized tools to precisely control beam amplitude, phase, and temporal properties. In this work, diffractive optical elements, specifically axicons and spiral phase plates, were employed to shape beam profiles, and characterization was performed using a beam profiler.

In this work, we demonstrate several examples of structured light applications in plasma spectroscopy. Three structured light types were utilized: Bessel beams for spatial structuring applied to confocal LIF, control of light over nonlinear trajectories in frequency space for wavelength modulation LIF, and vortex beams carrying orbital angular momentum for multidimensional LIF. These beam types made it possible to address challenges such as limited optical access and high background noise, while also enabling the extraction of multidimensional properties with a single laser beam.

#### A. Annular beam confocal LIF-ABC-LIF

A confocal approach was introduced into microscopy<sup>66</sup> and relies on optical arrangement where laser beam and collection optics share the same optical axis, and spatial resolution is achieved by point illumination with tightly focused laser beam and pinhole detection of the signal light to reject out-of-focus light. Although widely adopted in biological imaging or material diagnostics (e.g., confocal Raman<sup>67</sup>), confocal setups are less common in plasma research, where multiport access is often available and need for such approach is limited.

The achievable spatial resolution along the laser beam path largely depends on the depth of field (DoF) of the focused laser beam. This represents the primary limitation of the confocal approach in plasma diagnostics. Typically, plasma interrogation volumes are located far from the optics due to the presence of vacuum systems and related hardware. Consequently, the optical system's DoF significantly exceeds the characteristic dimensions of interest, such as plasma sheath thickness. Moreover, in single-photon LIF, the fluorescence signal scales linearly with laser intensity, causing light from out-of-focus regions to strongly degrade spatial resolution. Approaches like beam expansion or insertion of an obstructing disk have been tested to reduce the DoF or minimize the overlap between laser and fluorescence collection volumes. However, these methods resulted only in limited improvements to spatial resolution or cause reduction of signal-to-noise ratio (SNR) when finer resolution is required, as they maintained a Gaussian profile and focused mainly on manipulating collected fluorescence rather than the laser beam itself.

Annular (or Bessel) beams offer an alternative method to enhance resolution and reduce scattering. Generated using optical elements such as axicons, these beams exhibit radially varying intensity profiles. This characteristic allows distinct separation of the laser beam path from the fluorescence collection path, which is enclosed by the laser beam. Consequently, spatial resolution is fully governed by laser beam parameters and can be directly calculated using a straightforward formula for the DoF

$$DoF = \frac{4\lambda f}{\pi \delta} \frac{1}{\sin(\tan(R/f))},\tag{2}$$

where the annular beam with wavelength  $\lambda$ , radius R, and annulus thickness  $\delta$  is focused by the lens with a focus length f. For the setup used in this work,  $R \approx 11 \, \text{mm}$ ,  $\delta = 1.5 \, \text{mm}$ ,  $f = 300 \, \text{mm}$ , and  $\lambda = 668 \, \mathrm{nm}$ , the theoretical DOF is approximately 4.6 mm. However, real systems must account for nonuniform intensity distributions and optical aberrations, especially at greater focal distances. The laser beam intensity distribution near the focal point is shown in Fig. 4 and was reconstructed using a CMOS camera mounted on a movable stage (further details in Ref. 34). The fluorescence emission path was fully enclosed within the laser beam cone, effectively preventing overlap between excitation and collection paths. Furthermore, if a reflective wall is placed behind the interrogation volume, any back-reflected laser light diverges away from the collection optics, significantly reducing scattering and background signal. Figure 4 illustrates this arrangement. The laser-beam wavevector is indicated, while the collected fluorescence is depicted as a blue cone. The diagram highlights that the laser and collection paths are spatially separated, which minimizes scattered laser light and beam-wing contributions to the LIF signal.

### B. Wavelength-modulation LIF-WM-LIF

Another way to manipulate a laser beam is in a frequency space. In wavelength modulation spectroscopy (WMS),  $^{68,69}$  the laser wavelength is sinusoidally modulated around central frequency while slowly scanning across central absorption frequency  $\nu_0$ . This technique involves detecting and analyzing the modulated fluorescence signal at

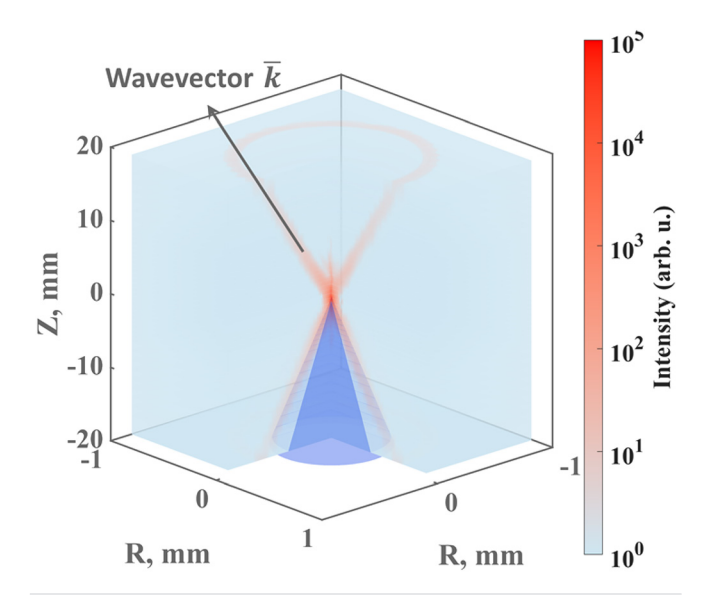


**FIG. 4.** Reconstructed 3D profile of focused annular beam. Note logarithmic intensity scale with most of the laser beam intensity within the focal spot. Arrow marks the direction of the wavevector. Blue cone marks the collected fluorescence cone, showing that laser beam paths and collected fluorescence light path are separated.

harmonics of the modulation frequency, typically the first or second harmonic. WMS enhances sensitivity to small spectral features by extracting the derivatives of the absorption profile. To It improves the signal-to-noise ratio by shifting the detection into a higherfrequency range, potentially reducing 1/f noise (at higher modulation frequencies), and provides a background-free signal, increasing the detector's dynamic range. The general schematic of the wavelength-modulated laser-induced fluorescence (WM-LIF) method is shown in Fig. 5. As the modulated laser beam (at frequency  $f_{mod}$ ) is scanned across a Doppler-broadened absorption profile, the resulting fluorescence signal carries both the absorption information and the modulation imprint. By selecting proper values of modulation amplitude  $\Delta\omega$  and  $f_{mod}$  it can be demonstrated that demodulation of the signal at the  $n^{th}$  harmonic of the  $f_{mod}$  isolates the nth derivative of the absorption line shape. This strategy differs from conventional amplitude-modulated (AM) LIF, in which the laser intensity is modulated at a fixed reference frequency or in a more complex way and after extracted from the collected signal. Fluorescence bearing the same AM signature is recovered from background noise with a lock-in amplifier referenced to that frequency, and the demodulated signal directly yields the VDF shape.

It is worth noting related approaches that use harmonic extraction. For example, Ref. 72 relies on heterodyne LIF detection that demodulates at the plasma oscillation (or drive) frequency to isolate the time-varying perturbation of the VDF, rather than recovering a spectral derivative via wavelength modulation. In contrast, wavelength-modulation LIF modulates the laser frequency and uses harmonic detection to measure derivatives of the fluorescence line, which boosts SNR and suppresses the baseline.

In the example shown in Fig. 5, the absorption profile consists of two Maxwellian VDFs, one centered at  $\omega$  and another shifted, partially overlapping with background emission. The presence of the second

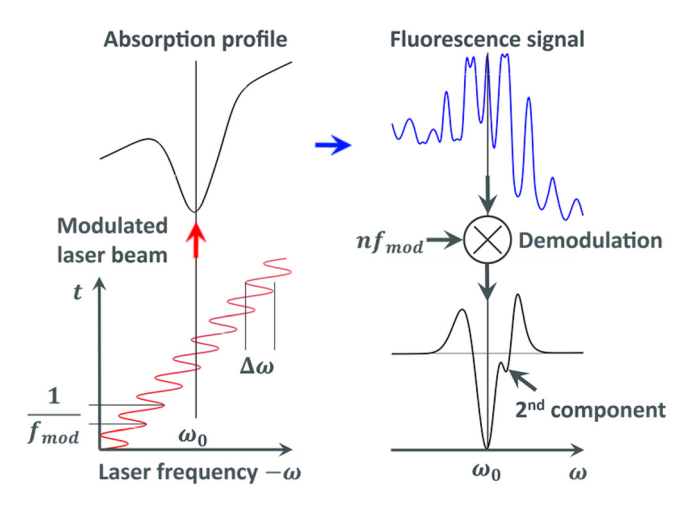


**FIG. 5.** Schematic of the wavelength-modulated laser-induced fluorescence (WM-LIF) approach. The laser frequency is sinusoidally modulated around the central absorption frequency  $\omega_0$  with the frequency  $1/f_{mod}$  and amplitude  $\Delta\omega$ . The modulated beam interacts with a Doppler-broadened absorption profile, generating a complex fluorescence signal. Demodulation of the fluorescence signal at a harmonic of the modulation frequency ( $nf_{mod}$ ). Frequency and amplitude of the modulation is not to scale. Absorption profile (top left) and its second derivative (bottom right) are theoretical estimation.

component becomes clearly visible in the second harmonic (second derivative) signal shown in the bottom right panel. More detailed descriptions of this technique and its application to laser-induced fluorescence measurements can be found in Ref. 35. The main motivation for using WM-LIF is to improve signal detection in noisy environments with strong background emissions and complex VDF shapes, which make accurate signal analysis difficult.

#### C. Vortex LIF

One key example of structured light is laser beams carrying OAM. In 1992, Allen et~al. showed  $^{73}$  that a light beam with a helical phase front carries a quantized OAM along its propagation axis, with each photon having angular momentum  $L_z=l\hbar$ , where l is the topological charge. Laguerre–Gaussian (LG) modes are standard examples, with wavefunctions containing  $\exp(il\phi)$  term, where  $\phi$  is the azimuthal coordinate. This azimuthal phase dependence twists the wavefront, causing the time-averaged Poynting vector to acquire an azimuthal component, leading the beam energy to spiral around the axis. The angle  $\beta$  between the Poynting vector and the axis at radial distance r is  $\beta = l/(kr)$ , where k is the axial wavevector magnitude. At r=0, the phase is undefined, producing a singularity and forming the characteristic doughnut-shaped intensity profile.

When an atom moves through a light beam, it experiences a Doppler shift determined by the rate at which the optical phase changes along its trajectory. For a conventional plane wave, this shift depends only on the component of atomic velocity along the beam's propagation direction as it is described by Eq. (1). A Laguerre–Gaussian beam carries OAM, and its phase varying along the beam axis as well as azimuthally is  $\Phi = kz + l\phi$ . This form assumes paraxial approximation and then curvature terms can be neglected, which is true in current work as collimated beam was used. An atom with

velocity components  $(V_{\phi},\ V_{Z})$  therefore samples two phase gradients:  $k\hat{z}$  and  $l\hat{\phi}$ . The frequency it perceives is shifted by

$$\Delta\omega_{LG} = -kV_z - lV_\phi/r. \tag{3}$$

The first term is the longitudinal Doppler shift. The second, the rotational (azimuthal) Doppler shift, is proportional to the OAM index l and inversely proportional to the radial distance r from the beam axis. The nature of this shift can be understood as follows. Revolution of the helical phase advances the field by l optical cycles, an atom with angular speed  $V_{\phi}/r$  detects an additional beat frequency  $lV_{\phi}/r$ . Figure 6 illustrates this concept: a particle crosses the helical wavefronts and experiences phase changes set by both axial and azimuthal geometry. Geometrically, the local Poynting vector traces a helix, and projecting the atomic velocity onto its axial and azimuthal directions yields the two Doppler contributions above.

The azimuthal Doppler shift enables extraction of more information with LIF diagnostics. In a vortex beam the resonant absorption frequency depends on both azimuthal velocity and radial position. When the laser carrier frequency plus the longitudinal and azimuthal Doppler terms matches the atomic resonance, excitation and fluorescence occur. Yoshimura *et al.* <sup>32,36</sup> first suggested applying this principle to plasma studies, demonstrating absorption <sup>74,75</sup> and fluorescence measurements and later it was suggested to be extended to full 3D velocity mapping. <sup>33</sup> In this work, we show an implementation of this method to measure the ion velocity-distribution function in an ion beam extracted from a plasma source.

#### IV. EXPERIMENTAL SETUP

Experiments were conducted using a plasma source (Fig. 7) from which ions can be extracted and accelerated. The plasma source is installed at the center of a standard 10-inch diameter six-way vacuum chamber. The chamber is pumped by a turbomolecular pump backed by a rough pump, maintaining a base pressure around 0.1  $\mu$ Torr. The plasma source is a rectangular metal box with a large area emitting cathode (2 cm in diameter), mounted on one of its side walls and

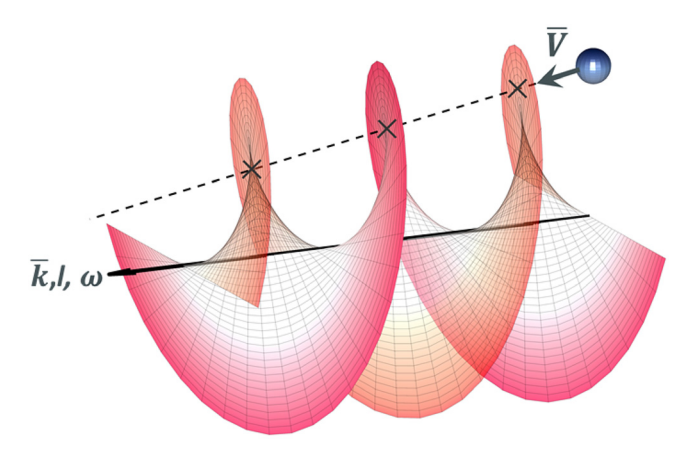


**FIG. 6.** Particle crossing a vortex laser beam with topological charge l=2. The particle moves with velocity  $\bar{v}$  relative to the beam wave-vector  $\bar{k}$  and crosses the helical wavefronts (black cross marks), experiencing a frequency  $\omega + \Delta \omega_{LG}$  shifted from the carrier  $\omega$ . The total shift combines the usual longitudinal term  $kV_z$  and an extra azimuthal term  $lV_{\phi}/r$ , which depends on the wavefront winding (topological charge l) and the particle's radial position r from the beam axis.

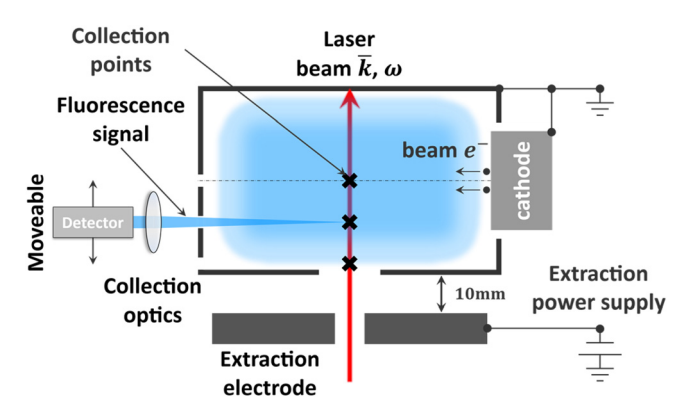


**FIG. 7.** General diagram of a plasma source and schematic for a conventional LIF collection scheme and marked collection points reachable for conventional optical arrangement. Schematic diagram of the plasma source and conventional LIF collection arrangement. Laser beam  $(\bar{k},\omega)$  is introduced through the front wall orifice. Fluorescence signals are collected at marked locations through sidewall openings. Dashed line shows the centerline.

electrically isolated from the grounded chamber walls. Gas enters the source through openings in the back wall, while ions exit through a circular opening on the front wall. A single extraction electrode positioned  $5-10 \, \text{mm}$  from this opening, biased up to  $-3 \, \text{kV}$ , extracts ions, forming an ion beam (Fig. 7).

During operation, the cathode is grounded, and the anode is positively biased. Most of the applied voltage drop occurs within the cathode sheath, a thin region near the cathode characterized by a strong electric field. Electrons emitted from the heated cathode are accelerated through this sheath, forming a beam-like electron population with energies determined by the difference between cathode and plasma potentials. These energetic electrons ionize neutral gas atoms through collisions, generating ions and lower-energy bulk electrons. Under such conditions, plasma inside the source is weakly collisional, with the ion mean-free path significantly exceeding the source dimensions  $(\lambda_i/L \gg 1)$ . Plasma exiting through the front opening becomes nearly collisionless.

Typical experimental conditions involved argon or xenon gases at flow rates of 1–5 sccm. During operation, pressures in the vacuum chamber ranged from 0.1 to 1 mTorr, as measured by an ion gauge, while pressures inside the source are estimated to be approximately ten times higher. Discharge voltages were typically 65–80 V, resulting in discharge currents of 1.5–2.0 A. Extraction voltage varied between 0 and  $-100\,\rm V.$ 

The selected plasma source imposes constraints on conventional laser-based diagnostics. It provides only a single front optical port, and a large cathode is a source of strong broadband emission with a drifting baseline. These conditions make the conventional orthogonal LIF geometry hard to implement and require more sensitive methods to recover the true VDF shape due to strong background emission. These constraints motivated the use of structured-light diagnostics. The operating regimes are standard for industrial plasma tools, and the source's pressure, power, and magnetic-field ranges are representative of related low-temperature plasma systems. The diagnostic approaches described here are transferable to other plasma devices (e.g., etching reactors, magnetrons).

The conventional laser-induced fluorescence (LIF) arrangement used in the experiments is illustrated in Fig. 7. A narrow-band laser beam, characterized by wavevector  $\bar{k}$  and frequency  $\omega$  is introduced into the plasma source through a 2 mm slit in the extractor plate and 10 mm diameter opening located on the front wall. Fluorescence photons are collected through three additional 3 mm diameter diagnostic ports positioned on the sidewall, providing measurements at different spatial positions along the laser beam axis. These collection points—designated as central (on the central line), middle, and edge (closes to the exit orifice)—correspond to different distances from the front wall opening, allowing spatially resolved plasma characterization, but only at three locations. More details on experimental arrangement, optical setups for ABC-LIF and WM-LIF diagnostics, as well as spatial localization of measurements are provided in the Appendix and can be found elsewhere.  $^{34,35}$ 

#### A. Vortex LIF setup

The vortex LIF setup uses a commercial, New Focus TLB-6917, tunable diode laser driven by a Vortex controller. 46 The laser operates at 834.95 nm central wavelength (in vacuum), delivers up to 60 mW, and light frequency can be tuned mode-hop-free for over 60 GHz with a linewidth below 300 kHz. A Toptica BoosTA-830 tapered amplifier boosts the laser power to 600 mW across the laser's tuning range. This laser was used to excite xenon ion (Xe II)  $5d[4]_{7/2} - 6p[3]_{5/2}$  transition at 834.953 nm in vacuum with fluorescence at 541.9 nm. After the amplifier, the beam intensity is modulated with mechanical chopper and passed through a spatial filter to ensure Gaussian profile. This is important as optical elements used for vortex beam generation are sensitive to laser beam shape imperfections. Laser beam is then passed through a removeable optical block consisting of two spiral phase plates, each with topological charge l=32, producing a vortex beam with total charge l = 64. Beam profiles measured with Coherent LaserCam-HR-II beam profiler camera before and after the plates are shown in Figs. 8(a) and 8(b) respectively.

The 6 mm-diameter vortex beam is then directed in the gap between the plasma source and the extractor plate [see Fig. 9(a)]. Fluorescence is collected through a narrow slit in the extractor by two plano–convex lenses and a pinhole for spatial filtering [Fig. 9(b)]. A PMT is used for signal detection, and its output is processed by a lockin amplifier referenced to the mechanical chopper that modulated the

laser. Light is collected from the upper edge of the laser column where the extracted ions move tangentially to the helical wavefronts; this geometry maximizes the azimuthal Doppler shift and thus the sensitivity to the orbital-angular-momentum component of the velocity distribution. Moreover, the azimuthal Doppler shift will cause modification of VDF only on one side, making it skewed. This allows to directly measure the parameters of azimuthal component in contrast with results presented in Ref. 32.

To test the effect of vortex beam on the shape of LIF signal measurements were repeated with the block of spiral phase plates removed, what resulted in a Gaussian beam of similar dimensions. All optical alignments and detector settings were left unchanged except for a minor adjustment of the collection optics to match the new beam center. Signals were acquired at applied acceleration voltages of  $V_{accel} = 0 \, V$  and  $V_{accel} = -50 \, V$  for both beam types. Assumption was made that the ion flow is uniform within the gap, and the small displacement required to re-center the Gaussian beam does not cause significant differences in velocity-distribution function. The paired data sets therefore provide a direct comparison between conventional and vortex LIF, allowing quantitative assessment of the azimuthal Doppler contribution. More details on selected experimental arrangement and reasoning for this will be provided in the section below.

#### V. RESULTS

Results from the three structured-light diagnostics, annular-beam confocal LIF (ABC-LIF), wavelength-modulation LIF (WM-LIF), and vortex-beam LIF, are summarized below. Detailed experimental procedures are reported elsewhere. The figures here present representative data that demonstrate the capabilities of each technique.

Comparison of ABC-LIF with conventional LIF is presented elsewhere. Where, we report new ABC-LIF data for plasma source operated with argon in several regimes. These measurements show one of the benefits of a confocal approach, as new optics geometry keeps the bright cathode out of the field of view, which improves SNR and enables more reliable retrieval of weak features. Figure 10 shows a representative VDF at Z=0.5 (Z=0 at the front wall, Z=1 at the back wall) for 2 sccm Ar and discharge voltage 55 V. The extractor plate was not installed. Negative velocity denotes flow toward the back wall along the laser wave vector (see Fig. 7). The signal was preprocessed by detrending with asymmetric least squares on Maxwellian distributions

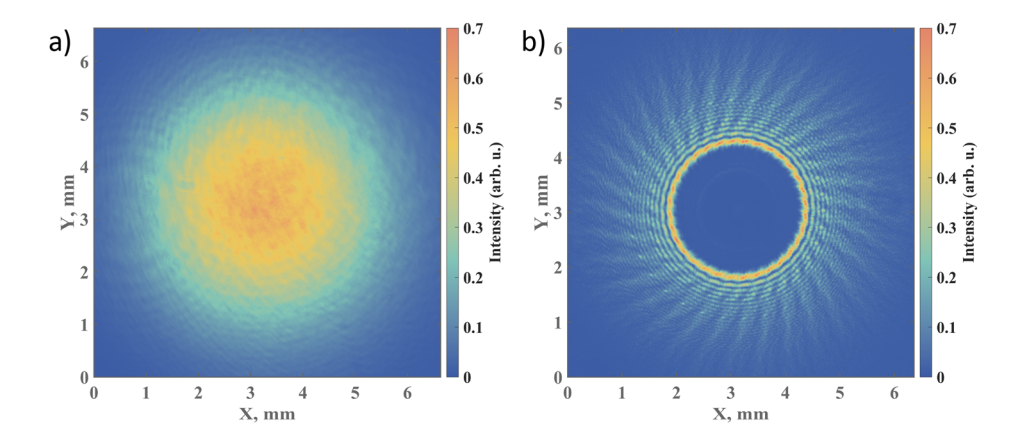


**FIG. 8.** Laser beam profiles (a) before the spiral phase plates; (b) after the second spiral phase plate with total topological charge I=64 Beam was focused with 200 mm lens and measurement was performed at 50 mm away from the lens in order to fit the beam onto the sensor of the beam profiler.

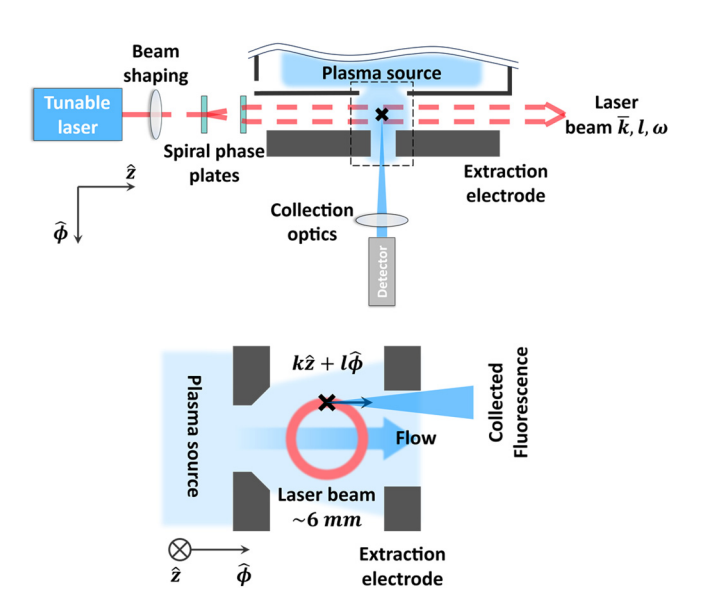


**FIG. 9.** General diagram of the vortex LIF experiment. (a) Top view of the setup. The vortex laser beam is generated with a pair of spiral phase plates with a total topological charge of l=64. Dashed box marks region shows in panel (b): side view of the setup. The light was collected from the top of the annular laser beam region to obtain VDF containing components along the laser beam direction and tangentially. PMT was used as a light detector.

to minimize  $\chi^2$  metric. Obtained VDF shows an interesting feature of bi-Maxwellian distribution with a slowly drifting bulk population  $V \approx -0.5 \pm 0.1 \, \mathrm{km/s}$  and  $T = 0.23 \pm 0.03 \, eV$ , and a cold, directed tail at  $V \approx -3.3 \pm 0.1 \, \mathrm{km/s}$  with  $T = 0.12 \pm 0.05 \, \mathrm{eV}$ . Langmuir probe measurements showed electron temperature of about 5 eV,

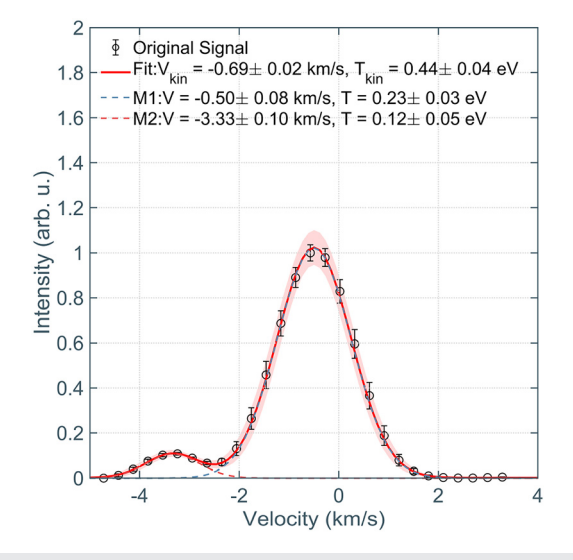


**FIG. 10.** Velocity distribution function of Ar ions at Z = 0.5, 2 sccm Ar, discharge voltage 55 V, B = 45 G (no extractor). Red line and shaded area are double-Maxwellian fit with 95% confidence interval. Fit parameters are shown in the legend.

which correspond to the Bohm velocity of  $v_{Bohm} \approx 3.5 \, \mathrm{km/s}$ , so the directed tail can be related to acceleration in presheath/sheath regions.

Figure 11 shows trends of ion velocities and temperatures of bulk and tail populations from the front opening (Z = 0) to the back wall along the laser beam (see Fig. 7). The bulk population drifts weakly toward the back wall across the cathode region, and its temperature stays nearly constant at  $\sim$  0.2–0.3 eV with modest rises near the walls. This indicates a small electric field (1-2 eV) that drives flow without significant ion heating. The fast 'tail' population shows more complex behavior. It is positive near the front wall with velocity  $\sim 2.5 \, \mathrm{km/s}$ , consistent with presheath/sheath acceleration (the Bohm speed is  $\sim$  3.5 km/s). The flow reverses sign near the beginning of the cathode region ( $Z \approx 0.2$ ) and then becomes increasingly negative toward the back wall. Both populations change their velocities by a similar amount, indicating they respond to the same axial field. The tail temperature remains low (0.1-0.2 eV) except for a local peak at the velocity sign change location. The observed sign change suggests a reversal of the axial electric field at the cathode-region boundary. A plausible cause of the weak ambipolar field is asymmetric electron loss to the front and back walls because the cathode is closer to the front wall. The exact origin of the tail requires further study. The measured VDF shows multiple ion populations and indicates complex processes inside the plasma source which would not be captured by conventional orthogonal LIF under the present access constraints.

Figures 12 and 13 present WM-LIF results for Ar ions. Spectra were recorded at two axial positions inside the source—center and mid-gap—each measured three times to establish statistics. All data were taken along the laser axis as shown in Fig. 7; the extractor plate was removed for these tests. The full optical layout and acquisition procedure are described in Ref. 35. Representative AM signals (red circles) and the corresponding WM signals (blue squares) are plotted with one-sigma envelopes.

The IVDF in Fig. 12(a) shows two distinct peaks at 0 km/s and -2.5 km/s. The WM signal in Fig. 11(b) exhibits matching features, indicating sensitivity to the same populations. AM and WM datasets were fitted with a sum of Maxwellians and a sum of second derivatives of Maxwellians respectively. The number of components varied from 1 to N. Using the  $\chi^2_{red}$  metric, the optimal fit was determined at N=2, confirming a bimodal IVDF; fitting details appear in Ref. 35. The agreement demonstrates that WM-LIF provides an independent validation of AM-based measurements while operating on a different detection principle.

Figure 13(a) displays the IVDF measured at the middle position, while Fig. 13(b) shows its second derivative. The IVDF is dominated by a central peak at 0 km/s with asymmetric wings. As before, both the AM and WM spectra were fitted with a sum of Maxwellians 1 to N and corresponding derivatives. Reference 35 reports that WM data are more sensitive to the fit than AM data, allowing to determine number of components N more reliably, this agrees with the model predictions (Sect. 3.1, Ref. 35). This enhanced sensitivity reveals three distinct populations at this location, providing deeper insight into the source's internal dynamics.

We present initial vortex-beam LIF results with the plasma source of Sec. IV. The goals were: (i) verify that a LIF signal for the selected Xe II transition can be obtained with a vortex beam, as some works report selection-rule changes;<sup>77–79</sup> and (ii) quantify changes in ion

b)

5

2.5

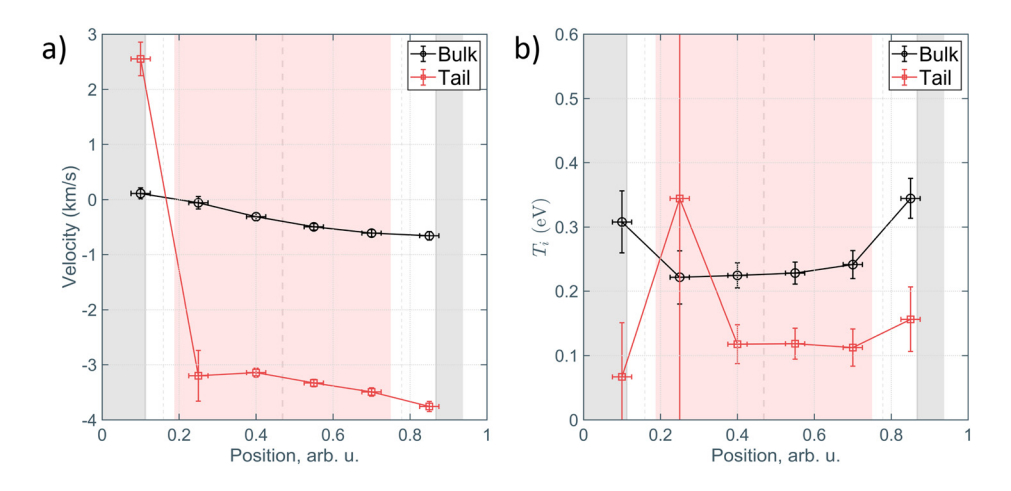
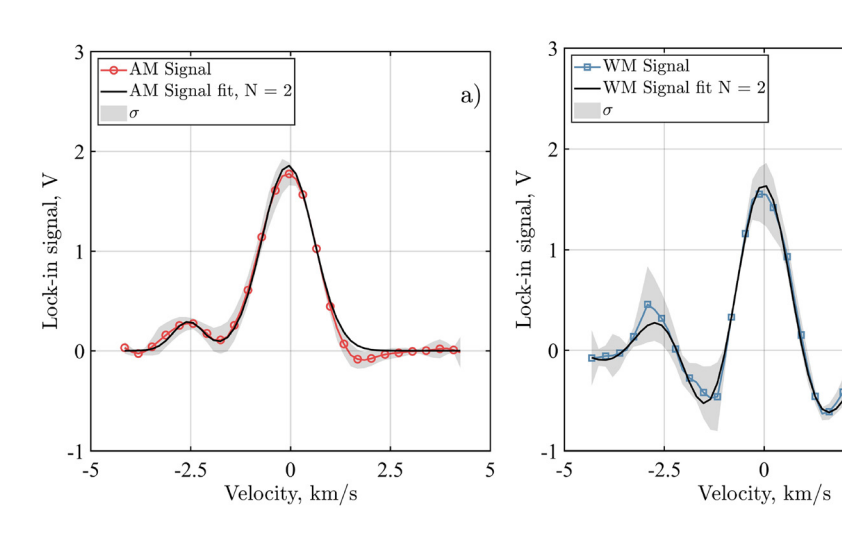


FIG. 11. Mean velocity (a) and ion temperature (b) of bulk (black) and tail (red) vs axial position Z. Negative velocity is toward the back wall (Z=1). Gray bands denote the front and back walls; the light-red band marks the cathode region. Vertical error bars are 95% confidence intervals of the fit; horizontal error bars show spatial resolution.



**FIG. 12.** The best fits of the (a) AM signal and (b) WM signal at the central location. *N* shows the number of Maxwellian distribution providing the optimal fit. Reproduced from Romadanov *et al.*, 35 with the permission of AIP Publishing.

VDF when switching between Gaussian and vortex beams, and when perpendicular flow is introduced by biasing the extractor. While no change in selection rules was expected for this transition due to its electric-dipole nature, possible contributions from higher order effects (quadrupole, etc.) remained unclear.

The 6 mm-diameter laser, either Gaussian or a vortex beam with topological charge l=64, was sent through the gap between the source and the extractor. Fluorescence was collected from the upper edge of the beam column so that only the velocities in the  $z-\phi$  plane contribute to the Doppler broadening, with the main contribution from the axial component along the beam [see Fig. 9(a)]. Four conditions were investigated: Gaussian beam with the acceleration voltage  $V_{accel}=0~V$ , Gaussian beam with  $V_{accel}=-50~V$ , vortex beam with  $V_{accel}=-50~V$ , and vortex beam at  $V_{accel}=-50~V$ . Eq. (3) gives the expected azimuthal Doppler shift (reported in GHz) due to the vortex component,  $\Delta \nu = l/r\sqrt{2eV_{accel}/M_i}$ . Assuming uniform induced flow in the gap, for l=64, r=3~mm, and  $V_{accel}=-50~V$ , the shift is  $\Delta \nu \approx 0.18~GHz$ . The longitudinal Doppler broadening of the 834.953 nm Xe II line at 0.3~eV is  $\approx 0.50~GHz$ , so the azimuthal

contribution should be observable, although its amplitude is reduced because the accelerated ion density is lower ( $nv \approx const$ ).

Figures 14(a)–14(d) show the measured VDFs with double-Gaussian fits (accounting for axial and azimuthal velocity components). Signals were preprocessed the same way as signal in Fig. 10. Since two velocity components scale differently, the initial analysis focused on quantifying changes in the VDF shape rather than separating each component explicitly. Following Yoshimura  $et\ al.$ ,  $^{32}$  the mean value  $\mu$ , standard deviation  $\sigma$ , and skewness  $\gamma$  were calculated with 95% confidence intervals.

The spectra obtained at  $V_{accel}=0~V$  with and without OAM are symmetric and have the same width  $\sigma$ . This shows: (i) the Xe II electric-dipole transition behaves as expected under an optical vortex (no selection-rule change), and (ii) there is no measurable flow toward the extractor in the probed region. Applying the extractor bias without OAM keeps the spectrum symmetric, indicating that any perpendicular velocity produced by the bias does not project on the direction of a Gaussian-beam wavevector and that no additional heating is introduced.

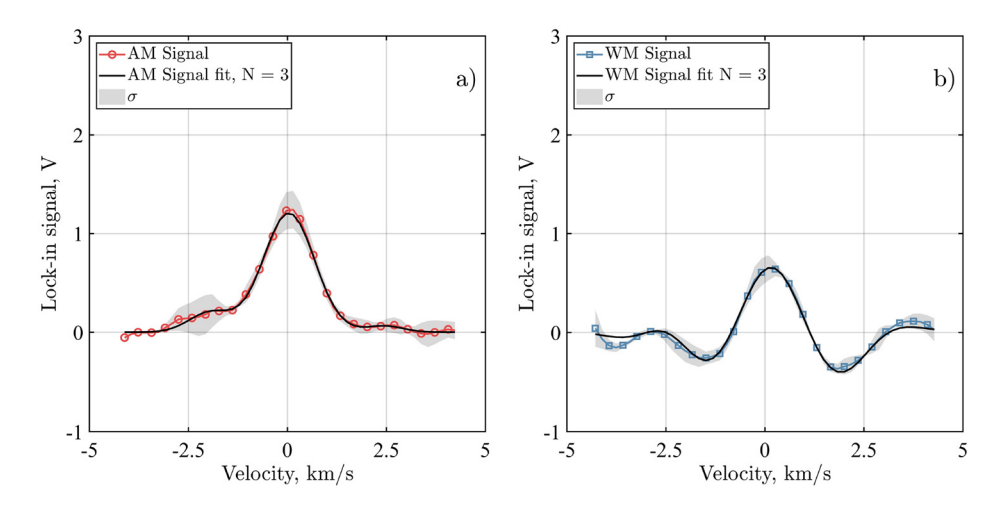


**FIG. 13.** The best fits of the a) AM signal and b) WM signal at the middle location. *N* shows the number of Maxwellian distribution providing the optimal fit. Reproduced from Romadanov *et al.*, <sup>35</sup> with the permission of AIP Publishing.

When OAM is combined with the extractor bias the VDF develops a positive skew  $\gamma$  and a larger apparent width  $\sigma.$  This is the signature of an added azimuthal Doppler term proportional to  $l/r\cdot V_\phi.$  The mean shift is larger than the simple estimate provided above. It is important to note that since the axial k and azimuthal l/r contributions scale differently,  $\sigma$  can no longer be interpreted directly as a temperature. While this discrepancy requires more detailed investigation, one of the possible explanations can be due to shift of the sampling

volume to the smaller radius, as  $\Delta \nu \sim 1/r$ . The data are consistent with  $r \sim 2$  mm, as compared to beam radius of  $r \sim 3$  mm which is possible as alignment error is about 1 mm.

In summary, data in Fig. 14 demonstrate that an optical vortex can be used to detect perpendicular ion velocity. The absence of any OAM effect at zero bias confirms that there are no modifications to selection-rules, while the OAM measurements with applied bias produces the expected VDF skew. A detailed comparison with

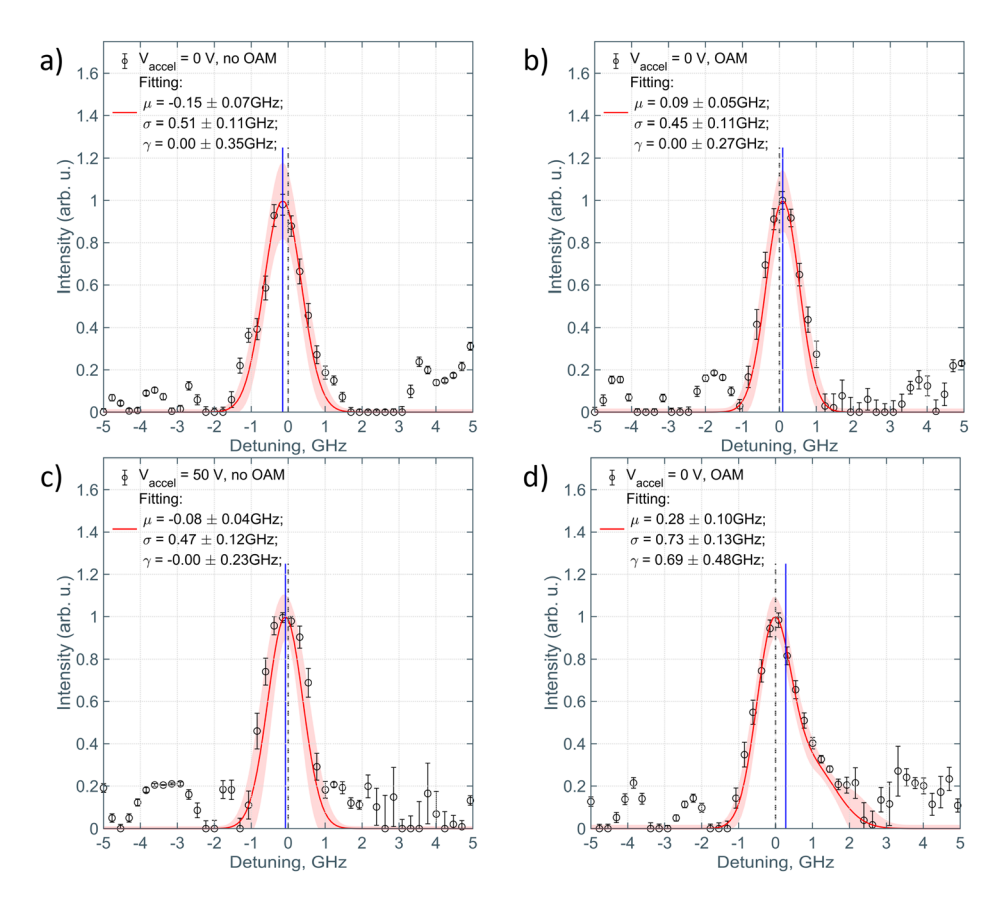


**FIG. 14.** lon-velocity distribution functions obtained by LIF under four probe/bias conditions. Symbols are experimental data; red curves are double-Gaussian fits with the extracted mean  $(\mu)$ , standard deviation  $(\sigma)$ , and skewness  $(\gamma)$  indicated, vertical dashed line shows 0 GHz shift, blue vertical line corresponds to  $\mu$ . (a) Gaussian beam,  $V_{accel}=0$  V. (b) Gaussian beam,  $V_{accel}=0$  V. (c) Vortex beam (l=64),  $V_{accel}=0$  V. (d) Vortex beam (l=64),  $V_{accel}=-50$  V. Positive detuning corresponds to velocities directed away from the plasma source.

conventional LIF and an investigation of the origin of this difference are planned.

#### VI. CONCLUSIONS

This work demonstrates how structured light can improve LIF diagnostics in industrial plasma devices relevant to nanofabrication of microelectronics, quantum information systems and magnetically confined fusion devices. We address three common limits: restricted optical access, complex signals in noisy backgrounds, and the need for multi-dimensional measurements that are often encountered in such systems. <sup>19,20</sup> By shaping the beam spatial, temporal (frequency), and phase profiles, we demonstrate LIF techniques that overcome these constraints.

ABC-LIF uses an axicon to form a ring beam and records ionvelocity data with about 5 mm spatial resolution at a 300 mm working distance. This resolution is comparable to that of orthogonal LIF yet requires only one optical port. The resolution can be further improved. The ring geometry allows adjustment of spatial resolution by changing the beam radius and lens focal length, keeps the excitation and collection paths separate, and prevents back-scattered laser light from the detector. The measured velocity distribution function is taken along the beam wave vector  $\bar{k}$ , which lies at a fixed angle to the optical axis set by the ring radius and focal distance. In this work, measurements show a key benefit of the confocal approach. The optics geometry keeps the bright cathode out of the field of view which improves SNR and enables more reliable retrieval of complex VDF profiles. It allowed detection of near-thermal bulk plus a cold, directed tail populations and track their changes within the source, indicating a complex internal field structure. This geometry is broadly useful for measurements normal to surfaces, for example across presheath/sheath regions, where its weakly diverging annular beam and coaxial collection minimize back reflections. It can be applied in ICP reactors and in Hall-thruster channels near the anode where side access is limited.

WM-LIF employs harmonic detection of a frequency-modulated laser to resolve complex velocity-distribution functions in noisy environments. The method detects multi-component features in the IVDFs that are not resolvable with standard amplitude-modulated LIF. WM-LIF therefore serves both as an independent check on AM-LIF measurements and as a robust option for extracting reliable data in high-noise environments. WM-LIF also pairs well with vortex LIF: its sensitivity to small line shape changes can improve detection of small azimuthal components, which are harder to resolve because (l/r) scaling for azimuthal Doppler shift is typically smaller than k [see Eq. (3)] scaling for axial component. In this way, even weaker transverse flows may be identifiable.

Building on previous experimental studies,  $^{32,33,36,74,75}$  vortex beams that carry orbital angular momentum were applied to LIF measurements. The helical wavefront produces an azimuthal Doppler shift proportional to the ion velocity component perpendicular to the beam and to the radial position. Tests with a vortex beam carrying l=64 showed a clear change in the IVDF when a transverse flow was present, in agreement with theory. These results indicate that a single vortex beam can provide multi-dimensional velocity data. Vortex LIF is broadly applicable where directed transverse flow exists, such as extraction regions and sheaths near biased surfaces, and it reduces the need for two beams or for normal-incidence access. A detailed analysis of the collected spectra will be presented in future work.

Tailoring the spatial, temporal, and phase structure of the probe beam in LIF diagnostics overcomes key experimental limits and yields more detailed measurements that open possibilities to directly study plasma processes in new environments and provide data for validation of computational codes and models. The three approaches demonstrated here can extend to other laser techniques, including Thomson and Raman scattering and line-of-sight absorption spectroscopy. This shows that applications of structured light in plasma diagnostics merit further study. Future work should examine how complex wavefronts interact with ground-state and excited species, determine whether they can access transitions that are not accessible now, and explore their ability to reveal other information (e.g., electric fields).

#### **ACKNOWLEDGMENTS**

The work was supported by the U.S. Department of Energy under CRADA agreement between PPPL and Applied Material Inc., entitled "Advanced Plasma Diagnostics for Characterization of Processing Reactors." The authors thank Dr. S. Kondeti and Dr. S. Yatom for assistance with the experimental setup and many helpful discussions; T. Bennett for technical support; Professor A. Smolyakov, N. Chopra, and S. H. Son for insightful conversations; and J. Kiviat and V. Gallegos for their help during internships.

## **AUTHOR DECLARATIONS**

#### **Conflict of Interest**

The authors have no conflicts to disclose.

#### **Author Contributions**

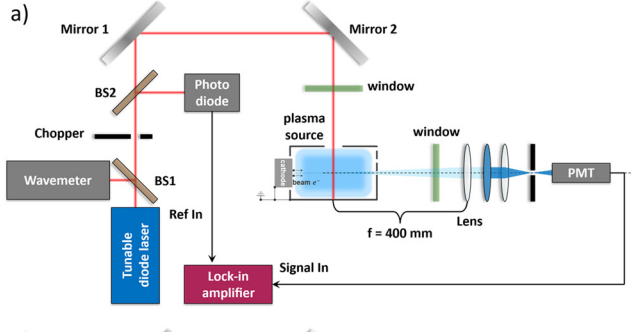
**Ivan Romadanov:** Writing – original draft (equal); Writing – review & editing (equal). **Yevgeny Raitses:** Writing – original draft (equal); Writing – review & editing (equal).

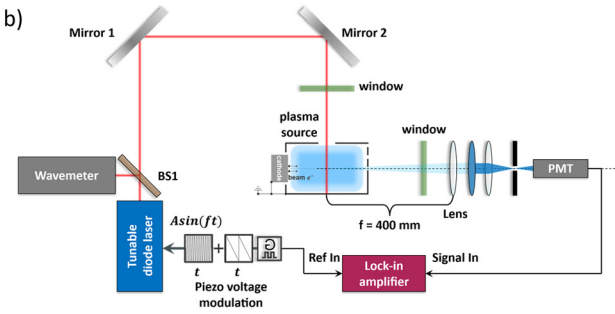
#### **DATA AVAILABILITY**

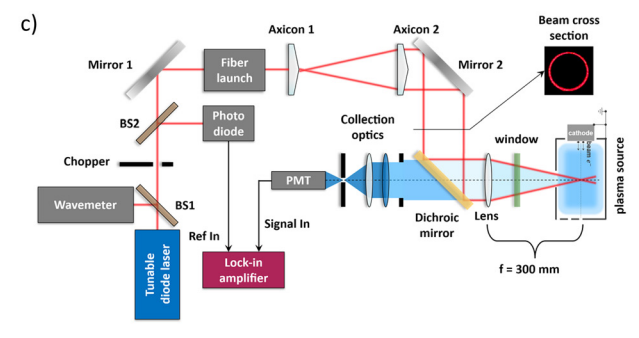
The data that support the findings of this study are available from the corresponding author upon reasonable request.

#### **APPENDIX: OPTICAL SETUPS**

General block diagrams of the conventional LIF, WM-LIF, and ABC-LIF arrangements are shown in Fig. 15. All three diagnostics share the wavemeter tap, the photodiode monitor (used for amplitude modulation), the lock-in amplifier, and the PMT detector. Two diode lasers were used depending on the probed species: a TOPTICA DLC Pro 670<sup>34</sup> for the argon transition and a TLB-6917 Vortex II<sup>46</sup> for the xenon transition. Confocal and WM-LIF diagnostics were implemented only with argon. Optical elements (mirrors, lenses, filters) were adjusted to the operating wavelength. Conventional and WM-LIF use the same side-view collection optics; switching between them replaces the mechanical chopper with a function generator to drive wavelength modulation. ABC-LIF uses the same laser injection path with an annular-beam module and collects fluorescence coaxially along the incident beam through the front port. Switching from conventional LIF to ABC-LIF required installing the annular-beam generation path and a new coaxial







 $\mbox{FIG. 15. Block diagrams of the (a) conventional LIF setup, (b) WM-LIF setup, and (c) ABC-LIF setup.} \label{eq:likelihood}$ 

collection path with a dichroic mirror. Comparison data were taken in sequential runs at identical discharge parameters; only the optical modules were swapped between runs. Concurrent operation of conventional LIF and ABC-LIF was not tested because only one PMT was available. With an additional detector, simultaneous collection normal to the beam and along the beam is possible. ABC-LIF was run in amplitude-modulation mode; wavelength-modulated ABC-LIF is planned.

#### **REFERENCES**

- <sup>1</sup>R. Engeln, B. Klarenaar, and O. Guaitella, "Foundations of optical diagnostics in low-temperature plasmas," Plasma Sources Sci. Technol. **29**, 063001 (2020).
- <sup>2</sup>A. R. Hanna and E. R. Fisher, "Investigating recent developments and applications of optical plasma spectroscopy: A review," J. Vac. Sci. Technol. A 38, 020806 (2020).
- <sup>3</sup>W. Demtröder, *Laser Spectroscopy* (Springer, Berlin, Heidelberg, 1996).
- <sup>4</sup>N. Sadeghi, "Practical aspects of molecular spectroscopy in plasmas 6. molecular spectroscopy techniques applied for processing plasma diagnostics," https://www.jstage.jst.go.jp/article/jspf/80/9/80\_9\_767/\_article.

- 5K. Muraoka and A. Kono, "Laser Thomson scattering for low-temperature plasmas," J. Phys. Appl. Phys. 44, 043001 (2011).
- 6M. I. Boulos, P. L. Fauchais, and E. Pfender, "Plasma diagnostics, optical emission and absorption spectroscopy," in *Handbook of Thermal Plasmas*, edited by M. I. Boulos, P. L. Fauchais, and E. Pfender (Springer International Publishing, Cham, 2023), pp. 963–1023.
- <sup>7</sup>S. Reuter, J. S. Sousa, G. D. Stancu, and J.-P. Hubertus van Helden, "Review on VUV to MIR absorption spectroscopy of atmospheric pressure plasma jets," Plasma Sources Sci. Technol. **24**, 054001 (2015).
- <sup>8</sup>R. A. Stern and J. A. Johnson, "Plasma Ion Diagnostics Using Resonant Fluorescence," Phys. Rev. Lett. **34**, 1548 (1975).
- <sup>9</sup>G. D. Severn, X. Wang, E. Ko, N. Hershkowitz, M. M. Turner, and R. McWilliams, "Ion flow and sheath physics studies in multiple ion species plasmas using diode laser based laser-induced fluorescence," Thin Solid Films 506–507, 674 (2006).
- <sup>10</sup>G. D. Severn, X. Wang, E. Ko, and N. Hershkowitz, "Experimental studies of the Bohm criterion in a two-ion-species plasma using laser-induced fluorescence," Phys. Rev. Lett. 90, 145001 (2003).
- <sup>11</sup>A. V. Gorbunov, E. E. Mukhin, E. B. Berik, K. Y. Vukolov, V. S. Lisitsa, A. S. Kukushkin, M. G. Levashova, R. Barnsley, G. Vayakis, and M. J. Walsh, "Laser-induced fluorescence for ITER divertor plasma," Fusion Eng. Des. 123, 695 (2017).
- <sup>12</sup>S. Mazouffre, "Laser-induced fluorescence diagnostics of the cross-field discharge of Hall thrusters," Plasma Sources Sci. Technol. 22, 013001 (2012).
- <sup>13</sup>M. B. Hopkins and J. F. Lawler, "Plasma diagnostics in industry," Plasma Phys. Controlled Fusion 42, B189 (2000).
- <sup>14</sup>C. J. Lorenzen, C. Carlhoff, U. Hahn, and M. Jogwich, "Applications of laser-induced emission spectral analysis for industrial process and quality control," J. Anal. At. Spectrom 7, 1029 (1992).
- <sup>15</sup>Y. J. Lee, H. J. Kwon, Y. Seok, and S. J. Hong, "IOT-based in situ condition monitoring of semiconductor fabrication equipment for e-maintenance," J. Qual. Maint. Eng. 28, 736 (2022).
- <sup>16</sup>N. B. Moore, W. Gekelman, P. Pribyl, Y. Zhang, and M. J. Kushner, "2-dimensional ion velocity distributions measured by laser-induced fluorescence above a radio-frequency biased silicon wafer," Phys. Plasmas 20, 083506 (2013).
- <sup>17</sup>L. Zhang, G. Tian, J. Li, and B. Yu, "Applications of absorption spectroscopy using quantum cascade lasers," Appl. Spectrosc. 68, 1095 (2014).
- <sup>18</sup>B. Jacobs, W. Gekelman, P. Pribyl, and M. Barnes, "Temporally resolved ion velocity distribution measurements in a radio-frequency plasma sheath," Phys. Plasmas 18, 053503 (2011).
- <sup>19</sup>G. S. Oehrlein, S. M. Brandstadter, R. L. Bruce, J. P. Chang, J. C. DeMott, V. M. Donnelly, R. Dussart, A. Fischer, R. A. Gottscho, S. Hamaguchi *et al.*, "Future of plasma etching for microelectronics: Challenges and opportunities," J. Vac. Sci. Technol. B 42, 041501 (2024).
- <sup>20</sup>D. B. Graves, C. B. Labelle, M. J. Kushner, E. S. Aydil, V. M. Donnelly, J. P. Chang, P. Mayer, L. Overzet, S. Shannon, S. Rauf *et al.*, "Science challenges and research opportunities for plasma applications in microelectronics," J. Vac. Sci. Technol. B **42**, 042202 (2024).
- <sup>21</sup>J. L. Santos, "Optical sensors for Industry 4.0," IEEE J. Sel. Top. Quantum Electron. 27, 1 (2021).
- <sup>22</sup>D. B. Graves, "Plasma processing," IEEE Trans. Plasma Sci. 22, 31 (1994).
- <sup>23</sup>S. Hamaguchi, "Plasma-surface interactions in material processing," J. Phys. Conf. Ser. 257, 012007 (2010).
- <sup>24</sup>V. M. Donnelly, "Plasma electron temperatures and electron energy distributions measured by trace rare gases optical emission spectroscopy," J. Phys. Appl. Phys. 37, R217 (2004).
- <sup>25</sup>H. Akatsuka, "Quantitative analysis of optical emission spectroscopy for plasma process monitoring," Jpn. J. Appl. Phys. 63, 050102 (2024).
- <sup>26</sup>R. Chen, H. Huang, C. J. Spanos, and M. Gatto, "Plasma etch modeling using optical emission spectroscopy," J. Vac. Sci. Technol. A 14, 1901 (1996).
- <sup>27</sup>S. Sridhar, L. Liu, E. W. Hirsch, V. M. Donnelly, and D. J. Economou, "Insights into the mechanism of in-plasma photo-assisted etching using optical emission spectroscopy," J. Vac. Sci. Technol. A 34, 061303 (2016).
- <sup>28</sup> A. Forbes, M. De Oliveira, and M. R. Dennis, "Structured light," Nat. Photonics 15, 253 (2021).
- <sup>29</sup>Y. Shen, X. Wang, Z. Xie, C. Min, X. Fu, Q. Liu, M. Gong, and X. Yuan, "Optical vortices 30 years on: OAM manipulation from topological charge to multiple singularities," Light Sci. Appl. 8, 90 (2019).

- <sup>30</sup>A. E. Willner, K. Pang, H. Song, K. Zou, and H. Zhou, "Orbital angular momentum of light for communications," Appl. Phys. Rev. 8, 041312 (2021).
- <sup>31</sup>M. Erhard, R. Fickler, M. Krenn, and A. Zeilinger, "Twisted photons: New quantum perspectives in high dimensions," Light Sci. Appl. 7, 17146 (2017).
- <sup>32</sup>S. Yoshimura, K. Terasaka, and M. Aramaki, "Application of optical vortex to laser-induced fluorescence velocimetry of ions in a plasma," J. Adv. Simul. Sci. Eng. 9, 150 (2022).
- 33K. Terasaka, S. Yoshimura, H. Minagawa, and M. Aramaki, "Three-dimensional flow velocity determination using laser-induced fluorescence method with asymmetric optical vortex beams," Sci. Rep. 14, 2005 (2024).
- <sup>34</sup>I. Romadanov and Y. Raitses, "A confocal laser-induced fluorescence diagnostic with an annular laser beam," Rev. Sci. Instrum. 94, 073002 (2023).
- <sup>35</sup>I. Romadanov, Y. Raitses, and A. Smolyakov, "Wavelength modulation laser-induced fluorescence for plasma characterization," Rev. Sci. Instrum. 95, 073516 (2024).
- <sup>36</sup>S. Yoshimura, K. Terasaka, and M. Aramaki, "Modification of laser-induced fluorescence spectrum by additional azimuthal Doppler effect in optical vortex beams," Jpn. J. Appl. Phys. 59, SHHB04 (2020).
- 37J. Vaudolon and S. Mazouffre, "Indirect determination of the electric field in plasma discharges using laser-induced fluorescence spectroscopy," Phys. Plasmas 21, 093505 (2014).
- <sup>38</sup>J. Pérez-Luna, G. J. M. Hagelaar, L. Garrigues, and J. P. Boeuf, "Method to obtain the electric field and the ionization frequency from laser induced fluorescence measurements," Plasma Sources Sci. Technol. 18, 034008 (2009).
- <sup>39</sup>E. L. Foley and F. M. Levinton, "Progress on the motional Stark effect with laser-induced fluorescence diagnostic (invited)," Rev. Sci. Instrum. 77, 10F311 (2006).
- <sup>40</sup>B. B. Ngom, T. B. Smith, W. Huang, and A. D. Gallimore, "Numerical simulation of the Zeeman effect in neutral xenon from NIR diode-laser spectroscopy," J. Appl. Phys. **104**, 023303 (2008).
- <sup>41</sup>D. S. Thompson, T. E. Steinberger, A. M. Keesee, and E. E. Scime, "Laser induced fluorescence of Ar-I metastables in the presence of a magnetic field," Plasma Sources Sci. Technol. 27, 065007 (2018).
- <sup>42</sup>M. Sackers, O. Marchuk, D. Dipti, Y. Ralchenko, S. Ertmer, S. Brezinsek, and A. Kreter, "Zeeman effect of isotopes of Kr and Xe investigated at the linear plasma device PSI-2," Plasma Sources Sci. Technol. 33, 025015 (2024).
- 43H. F. Döbele, U. Czarnetzki, and A. Goehlich, "Diagnostics of atoms by laser spectroscopic methods in plasmas and plasma-wall interaction studies (vacuum ultraviolet and two-photon techniques)," Plasma Sources Sci. Technol. 9, 477 (2000).
- <sup>44</sup>V. S. S. K. Kondeti, S. Yatom, I. Romadanov, Y. Raitses, L. Dorf, and A. Khomenko, "Report on laser-induced fluorescence transitions relevant for the microelectronics industry and sustainability applications," J. Vac. Sci. Technol. A 42, 063005 (2024).
- <sup>45</sup>G. D. Severn, D. A. Edrich, and R. McWilliams, "Argon ion laser-induced fluorescence with diode lasers," Rev. Sci. Instrum. 69, 10 (1998).
- <sup>46</sup>P. Svarnas, I. Romadanov, A. Diallo, and Y. Raitses, "Laser-induced fluorescence of Xe I and Xe II in ambipolar plasma flow," IEEE Trans. Plasma Sci 46, 3998 (2018).
- <sup>47</sup>C. V. Young, A. Lucca Fabris, and M. A. Cappelli, "Ion dynamics in an E × B Hall plasma accelerator," Appl. Phys. Lett. 106, 044102 (2015).
- <sup>48</sup>S. Hotta, "Optical transition and selection rules," in *Mathematical Physical Chemistry: Practical and Intuitive Methodology*, edited by S. Hotta (Springer Nature, Singapore, 2023), pp. 127–153.
- <sup>49</sup> M. J. Goeckner, J. Goree, and T. E. Sheridan, "Saturation broadening of laser-induced fluorescence from plasma ions," Rev. Sci. Instrum. 64, 996 (1993).
- <sup>50</sup>O. V. Angelsky, A. Y. Bekshaev, S. G. Hanson, C. Y. Zenkova, I. I. Mokhun, and J. Zheng, "Structured light: Ideas and concepts," Front. Phys 8, 114 (2020).
- <sup>51</sup>M. Duocastella and C. b Arnold, "Bessel and annular beams for materials processing," Laser Photonics Rev. 6, 607 (2012).
- 52 A. M. Yao and M. J. Padgett, "Orbital angular momentum: Origins, behavior and applications," Adv. Opt. Photonics 3, 161 (2011).
- 53C. He, Y. Shen, and A. Forbes, "Towards higher-dimensional structured light," Light Sci. Appl. 11, 205 (2022).
- 54]. Mertz, "Optical sectioning microscopy with planar or structured illumination," Nat. Methods 8, 811 (2011).
- <sup>55</sup>H. Rubinsztein-Dunlop, A. Forbes, M. V. Berry, M. R. Dennis, D. L. Andrews, M. Mansuripur, C. Denz, C. Alpmann, P. Banzer, T. Bauer *et al.*, "Roadmap on structured light," J. Opt 19, 013001 (2017).

- <sup>56</sup>A. Li, S. Chai, H. Peng, Z. Zhao, J. Ren, and W. Wu, "Laser-induced breakdown spectroscopy using 2D structured light: A case of spectral signal enhancement on metal samples," Anal. Chem. 97, 3253 (2025).
- <sup>57</sup>G. Pesce, P. H. Jones, O. M. Maragò, and G. Volpe, "Optical tweezers: Theory and practice," Eur. Phys. J. Plus 135, 949 (2020).
- 58 S. Slussarenko and G. J. Pryde, "Photonic quantum information processing: A concise review," Appl. Phys. Rev. 6, 041303 (2019).
- <sup>59</sup>F. M. Levinton and F. Trintchouk, "Visualization of plasma turbulence with laser-induced fluorescence (invited)," Rev. Sci. Instrum. 72, 898 (2001).
- <sup>60</sup>M. Burger, P. Polynkin, and I. Jovanovic, "Filament-induced breakdown spectroscopy with structured beams," Opt. Express 28, 36812 (2020).
- 61 J. Wang and Y. Liang, "Generation and detection of structured light: A review," Front. Phys. 9, 688284 (2021).
- <sup>62</sup>Y. Shen, Q. Zhan, L. G. Wright, D. N. Christodoulides, F. W. Wise, A. E. Willner, K. Zou, Z. Zhao, M. A. Porras, A. Chong *et al.*, "Roadmap on spatio-temporal light fields," J. Opt. 25, 093001 (2023).
- <sup>63</sup>C. Maurer, A. Jesacher, S. Bernet, and M. Ritsch-Marte, "What spatial light modulators can do for optical microscopy," Laser Photonics Rev. 5, 81 (2011).
- E. Mikheeva, C. Kyrou, F. Bentata, S. Khadir, S. Cueff, and P. Genevet, "Space and time modulations of light with metasurfaces: Recent progress and future prospects," ACS Photonics 9, 1458 (2022).
  M. Sumetsky, B. J. Eggleton, and P. S. Westbrook, "Holographic methods for phase
- <sup>65</sup>M. Sumetsky, B. J. Eggleton, and P. S. Westbrook, "Holographic methods for phase mask and fiber grating fabrication and characterization," in *Laser Micromachining* for Optoelectronic Device Fabrication (SPIE, 2003), Vol. 4941, pp. 1–15.
- for Optoelectronic Device Fabrication (SPIE, 2003), Vol. 4941, pp. 1–15.

  66W. b Amos and J. g White, "How the confocal laser scanning microscope entered biological research," Biol. Cell 95, 335 (2003).
- 67P. Vinchon, X. Glad, G. Robert-Bigras, R. Martel, A. Sarkissian, and L. Stafford, "A combination of plasma diagnostics and Raman spectroscopy to examine plasma-graphene interactions in low-pressure argon radiofrequency plasmas," J. Appl. Phys. 126, 233302 (2019).
- <sup>68</sup>J. M. Supplee, E. A. Whittaker, and W. Lenth, "Theoretical description of frequency modulation and wavelength modulation spectroscopy," Appl. Opt. **33**, 6294 (1994).
- <sup>69</sup>G. C. Mathews and C. S. Goldenstein, "Wavelength-modulated planar laser-induced fluorescence for imaging gases," Opt. Lett. 42, 5278 (2017).
- <sup>70</sup>D. G. Cameron and D. J. Moffatt, "A Generalized Approach to Derivative Spectroscopy," Appl. Spectrosc. 41, 539 (1987).
- 71 E. E. Scime, J. Freeze, T. J. Gilbert, and T. E. Steinberger, "Laser induced fluorescence using frequency modulated light," Rev. Sci. Instrum. 95, 083550 (2024).
- <sup>72</sup>A. Diallo, S. Keller, Y. Shi, Y. Raitses, and S. Mazouffre, "Time-resolved ion velocity distribution in a cylindrical Hall thruster: Heterodyne-based experiment and modeling," Rev. Sci. Instrum. 86, 033506 (2015).
- 73L. Allen, M. W. Beijersbergen, R. J. C. Spreeuw, and J. P. Woerdman, "Orbital angular momentum of light and the transformation of Laguerre-Gaussian laser modes," Phys. Rev. A 45, 8185 (1992).
- 74H. Minagawa, S. Yoshimura, K. Terasaka, and M. Aramaki, "Analysis of azimuthal Doppler shift of anisotropically absorbed Laguerre-Gaussian beam propagating in transverse flow," Plasma Fusion Res. 17, 1401099 (2022).
- 75H. Minagawa, S. Yoshimura, K. Terasaka, and M. Aramaki, "Data-volume reduction of optical vortex laser absorption spectroscopy by coarse-graining using a quadrant photodiode," Jpn. J. Appl. Phys. 63, 056002 (2024).
- 76J. Peng, S. Peng, A. Jiang, J. Wei, C. Li, and J. Tan, "Asymmetric least squares for multiple spectra baseline correction," Anal. Chim. Acta 683, 63 (2010)
- <sup>77</sup>C. T. Schmiegelow, J. Schulz, H. Kaufmann, T. Ruster, U. G. Poschinger, and F. Schmidt-Kaler, "Transfer of optical orbital angular momentum to a bound electron," Nat. Commun. 7, 12998 (2016).
- <sup>78</sup>M. Babiker, C. R. Bennett, D. L. Andrews, and L. C. Dávila Romero, "Orbital angular momentum exchange in the interaction of twisted light with molecules," Phys. Rev. Lett. 89, 143601 (2002).
- <sup>79</sup>C. T. Schmiegelow, J. Schulz, H. Kaufmann, T. Ruster, U. G. Poschinger, and F. Schmidt-Kaler, "Excitation of an atomic transition with a vortex laser beam," arXiv:1511.07206 (2015).
- <sup>80</sup> A. Savitzky and M. J. E. Golay, "Smoothing and differentiation of data by simplified least squares procedures," Anal. Chem 36, 1627 (1964).